

Available online at www.sciencedirect.com

jmr&t
Journal of Materials Research and Technology
journal homepage: www.elsevier.com/locate/jmrt



Original Article

Investigation into the influence of CNTs configuration on the thermal expansion coefficient of CNT/Al composites



Li Zhou^b, Kuanyu Liu^b, Tiebing Yuan^b, Zhenyu Liu^a, Quanzhao Wang^{a,*},
Bolü Xiao^a, Zongyi Ma^a

^a Institute of Metal Research, Chinese Academy of Sciences, Shenyang 110016, PR China

^b School of Electromechanical and Automotive Engineering, Yantai University, Yantai 264005, PR China

ARTICLE INFO

Article history:

Received 6 March 2022

Accepted 6 April 2022

Available online 11 April 2022

Keywords:

Representative volume element

Thermal expansion coefficient

CNT/Al composites

Configuration

Orientation

ABSTRACT

A 3D representative volume element (RVE) model was developed to analyze the effective thermal expansion coefficient (CTE) of carbon nanotube reinforced aluminum (CNT/Al) composites. The influences of geometric configuration, orientation and volume fraction of CNTs on CTE of the CNT/Al composites were investigated. The results show that the orientation of CNTs significantly influences the stress and strain distributions around CNTs, and when CNTs are parallel to the load direction, the constraint effect of CNTs on the matrix is the largest. Furthermore, the configuration of CNTs also plays an important role in reducing thermal expansion behavior of CNT/Al composites, and the bundled configuration exhibit the lowest CTE. In particular, with the increase of the number of CNTs in each bundle, the CTE decreases and then tends to be unchanged. When the volume fraction of CNTs is 5%, and the number of CNTs in each bundle is 25, the CTE of the composite reaches $5.12 \times 10^{-6}/^{\circ}\text{C}$, which is 76% lower than the CTE of the matrix. A linear decrease of the CTE of CNT/Al composites is observed as the CNT volume fraction increases. Overall, this work establishes a comprehensive understanding of factors affecting the CTE, and the obtained findings could provide a good theoretical basis for designing low CTE CNT/Al composites.

© 2022 The Authors. Published by Elsevier B.V. This is an open access article under the CC BY license (<http://creativecommons.org/licenses/by/4.0/>).

1. Introduction

Metal matrix composites have high stiffness and strength, excellent thermal stability and strong designability, which are widely used in the aerospace, automobile structure, thermal

and electrical transmission, electronics etc. [1–4]. However, for the ceramic reinforced metal matrix composites, increase of the volume fraction and size of the ceramic reinforcements, the application of these materials is restricted by their difficulty to machine. Carbon nanotube (CNT) has

* Corresponding author.

E-mail address: qzhwang@imr.ac.cn (Q. Wang).

<https://doi.org/10.1016/j.jmrt.2022.04.042>

2238-7854/© 2022 The Authors. Published by Elsevier B.V. This is an open access article under the CC BY license (<http://creativecommons.org/licenses/by/4.0/>).

extremely low thermal expansion coefficient (CTE ≈ 0/K), superior mechanical strength and thermal conductivity. It is one of the ideal reinforcements for the preparation of the high-performance composites with high thermal conductivity and tailored CTE.

Compared with ceramic/metal composites, a superior class of composites can be prepared by adding a small amount of CNTs to the metal materials. For example, the modulus of aluminum matrix composites with 3 vol.% CNTs can reach 90 GPa and the strength can reach 600 MPa, which is equivalent to the properties of aluminum matrix composites with 20–25 vol.% SiC [5]. Yang et al. [6] reported that increased CNT content (up to 4.5 wt%) improved the mechanical properties of CNT/Al composites, and 4.5 wt% CNT/Al composites exhibited the largest hardness and tensile strength, which was 2.3 and 2.4 times higher than that of starting Al, respectively. In addition, the dispersion, particularly non-uniform dispersion of the CNTs in the matrix plays a crucial role for mechanical and thermal properties of the composite [7,8]. Because the CTE varies inversely with the Young's modulus, CNT has a very low or even negative CTE, in the range -2×10^{-5} - $0.5 \times 10^{-5} \text{ K}^{-1}$ depending on the CNT characteristics [9]. Therefore, it is expected that the combination of CNTs with metal materials will make it possible to fabricate composites with low CTE.

Owing to the difficulty in incorporating a high content of CNTs into the aluminum matrix, most research efforts have focused on the composites within 5 wt% CNTs [10–12]. Several studies have reported that the CTE decreased significantly with the increase of CNT content in Al matrix [6,11–16], and this is because CNTs effectively constrains the thermal expansion of Al matrix [17]. Liu et al. [11] showed that the CTE decreased by about 9.3% and 29%, respectively, for the 1.5 vol.% and 4.5 vol.% CNT/2009Al composites.

In addition, most of published data showed that the CTE of CNT/Al composites varies greatly even with the same CNT content: a 17% decrease for 4.5 wt% CNT/Al composites [6], a 12% reduction for 1.28 vol.% CNT/2024Al composites [18], a 30% decrease for 2 wt% CNT/Al composites [15], and a 30% decrease for 5 wt% CNT/Al composites [16]. Particularly, Tang et al. [17] reported the most significant reduction in CTE by 65% of CNT/Al composites with 15 vol.% single-walled carbon nanotubes. Moreover, the CNT/Al composites with aligned CNTs exhibited much lower CTE compared with those with randomly oriented CNTs [13]. This indicates that CNTs, especially the aligned CNTs could effectively constrain the thermal expansion of the aluminum matrix.

The CTE of CNT/Al composites is influenced by various factors, such as the microstructure, distribution and orientation of CNTs, and interface, etc. To predict the CTE of CNT/Al composites, the widely used models are the rule of mixtures (ROMs) and Turner's model. Unfortunately, the experimental results are not often consistent with those predicted by the theory models. The reason is that most of the theory models only consider the influence of filler content and simplified shapes of fillers, ignore the effect of microstructure, such as interface, distribution or orientation of CNTs in matrix, and complex defect structures, etc.

Finite element (FE) analysis is increasingly applied to predict the properties of composites and accelerate design of new composites. Through FE simulation with a limited experiments

for verification, the properties of the composites can be predicted accurately and effectively, where the traditional sole mechanical testing cannot or hardly work [19,20]. Yang et al. [21] have investigated the influence of the angle of graphite on thermal properties of graphite reinforce Cu matrix composite, and reported that the thermal conductivity of composite can be improved with the addition of graphite which has the improved orientation distribution. The result of the simulated thermal conductivity is as same as the measured thermal conductivity. However, up to now, the influence of CNT configurations on the CTE of CNT/Al composites has seldom comprehensively analyzed in literatures yet. Therefore, in order to achieve high prediction accuracy of CTE of CNT/Al composites, a thorough understanding the influence of CNT configurations on the CTE is necessary.

As well known, alignment of CNTs into a metal matrix is very challenging and the configurations of CNTs depend on the preparation route. Although, several typical CNT configurations may simultaneously exist in the matrix, and various processing techniques have been explored for fabrication CNT/Al composites with layered [22,23], bundled [24], directionally aligned [5], and mostly randomly arranged configurations of CNTs. In this work, a 3D representative volume element (RVE) with five typical CNT configurations was established to study the CTE of CNT/Al composites. In order to offer an accurate representation of real configuration, the anisotropy, volume fraction of CNTs, and interface were considered.

2. Computation of the effective CTE

The effective CTE of all RVE can be calculated using following expression:

$$a_{ij} = \frac{\bar{\epsilon}_{ij} \delta_{ij}}{\Delta T} \quad i \text{ and } j = x, y, z \quad (1)$$

where δ_{ij} is the Kronecker symbol and if $i = j$, then $\delta_{ij} = 1$, else $\delta_{ij} = 0$. ΔT is the temperature difference loading from the reference temperature. $\bar{\epsilon}_{ij}$ is the average strain component of the RVE in the corresponding direction, and the average strain can be calculated by:

$$\bar{\epsilon}_{ij} = \frac{1}{V} \left[\int_{v_c} \epsilon_{ij}^c dv_c + \int_{v_m} \epsilon_{ij}^m dv_m + \int_{v_i} \epsilon_{ij}^i dv_i \right] \quad (2)$$

where, V is the total volume of CNT/Al composites, ϵ_{ij}^c , ϵ_{ij}^m and ϵ_{ij}^i are the local variations of strain in CNTs, matrix and interface, respectively. Similarly, v_c , v_m and v_i are the local volumes of CNTs, matrix and interface, respectively.

In the elastic regime, the thermo-elastic properties of the matrix and interface are considered isotropic, and the elastic strain is related to the stress by the Generalized Hooke's law:

$$\sigma'_{ij} = [D]_{ijkl} \epsilon'_{ij} \quad (3)$$

where, σ'_{ij} and ϵ'_{ij} are the stress and strain components, i indicates the direction normal to plane, and j indicates the direction of component. $[D]_{ijkl}$ is the fourth-order elasticity tensor.

$$\epsilon'_{ij} = [C]_{i'j'k'l'} \sigma'_{ij} \tag{4}$$

where, $[C]_{i'j'k'l'}$ is the compliance matrix of $[D]_{i'j'k'l'}$.

In contrast, the thermo-elastic properties of CNTs are considered anisotropic along the axis and radius directions, and CNTs are assumed to be transversely isotropic, as shown in Fig. 1. $E_{11} = E_{22} = E_r$, $\nu_{31} = \nu_{32} = \nu_{ar}$, $\nu_{13} = \nu_{23} = \nu_{ra}$, $G_{13} = G_{23} = G_a$, where r and a stand for “radius” and “axis” directions of CNTs, respectively. Thus, while ν_{ar} has the physical interpretation of the Poisson's ratio that characterizes the strain in the plane of isotropy resulting from stress normal to it, ν_{ra} characterizes the axis strain in the direction normal to the plane of isotropy resulting from stress in the plane of isotropy. In general, the quantities ν_{ar} and ν_{ra} are not equal and are related by $\frac{\nu_{ar}}{E_a} = \frac{\nu_{ra}}{E_r}$. The stress-strain laws reduce to

$$[\epsilon]^c = \begin{bmatrix} \epsilon_{11} \\ \epsilon_{22} \\ \epsilon_{33} \\ \gamma_{12} \\ \gamma_{13} \\ \gamma_{23} \end{bmatrix} = \begin{bmatrix} \frac{1}{E_r} & \frac{\nu_r}{E_r} & \frac{\nu_{ar}}{E_a} \\ \frac{\nu_r}{E_r} & \frac{1}{E_r} & \frac{\nu_{ar}}{E_a} \\ \frac{\nu_{ra}}{E_r} & \frac{\nu_{ra}}{E_r} & \frac{1}{E_a} \\ & & & \frac{1}{G_r} \\ & & & & \frac{1}{G_a} \\ & & & & & \frac{1}{G_a} \end{bmatrix} \begin{bmatrix} \sigma_{11} \\ \sigma_{22} \\ \sigma_{33} \\ \tau_{12} \\ \tau_{13} \\ \tau_{23} \end{bmatrix} = [C]_{i'j'k'l'}^c [\sigma]^c \tag{5}$$

where, $G_r = E_r / 2(1 + \nu_r)$. Therefore, there are only 5 independent material parameters to calculate the stiffness of CNTs.

In micro-scale, CNTs are often randomly distributed in the RVE, and the effect of the CNT orientation should be considered. Here, a local coordinate system O123 is adopted and is attached to CNTs. In the FE calculation, the thermo-elastic

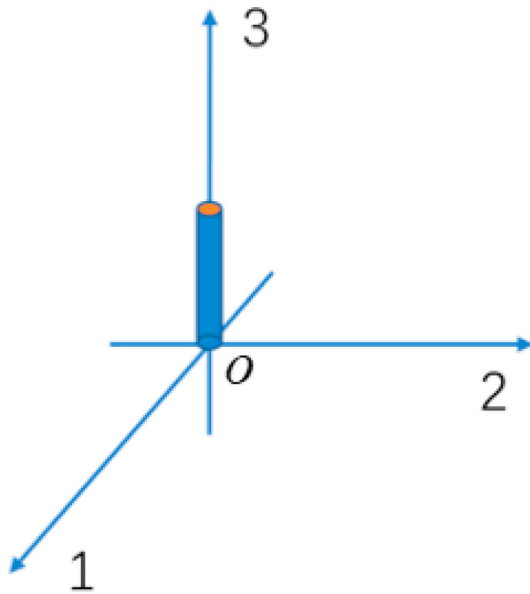


Fig. 1 – Orientation vector of a spatially oriented CNT.

tensor of CNT should be transformed from its local coordinate system to the global coordinate system. A convenient and practical way of parameterizing the orientation of a CNT in a 3D space is using two angles [25], as it is shown in Fig. 2.

The stress-strain relationship in the global coordinate system can be obtained by the rotation transformation of the stress-strain relationship in the material local coordinate system.

In Fig. 2, p is a unit vector representing the CNT orientation, which can be expressed as $p = (\cos \theta, \sin \theta \cos \varphi, \sin \theta \sin \varphi)$. Where θ and φ are the Euler angles as shown in Fig. 2. x, y and z are the three directions of the global coordinate. We denoted u_i and u'_j as the unit vectors of the global coordinate ($0, x, y,$ and z) and local coordinate ($0, 1, 2,$ and 3), respectively. A relationship between them can be constructed as follows [25]:

$$u_i = T_{ji} u'_j \tag{6}$$

Then, transformation matrix T_{ji} is expressed in terms of the angles from the local coordinate system unit base vector to the global coordinate system, which is obtained as:

$$T_{ji} = \begin{bmatrix} \cos \varphi \cos \theta & -\sin \varphi & \cos \varphi \sin \theta \\ \sin \varphi \cos \theta & \cos \varphi & \sin \varphi \sin \theta \\ -\sin \theta & 0 & \cos \theta \end{bmatrix} \tag{7}$$

Therefore, for the case of perfectly aligned CNTs, we obtained the elastic tensor $[C]_{ijkl}$ and effective CTE tensor α_{ij} of CNTs in the global coordinate from the local coordinate system. They can be given by [26]:

$$[C]_{ijkl}^c = T_{eifjgkhl} [C]_{i'j'k'l'}^c, \text{ where } T_{eifjgkhl} = T_{ei} \otimes T_{fj} \otimes T_{gk} \otimes T_{hl} \tag{8}$$

$$\alpha_{ij}^c = T_{eifj} \alpha_{ef}^c, \text{ where } T_{eifjgkhl} = T_{ei} \otimes T_{fj} \tag{9}$$

In the FE code ABAQUS, the thermal elastic tensors can be transformed from their local coordinate to the global coordinate by activating the ‘Material Orientation’ option.

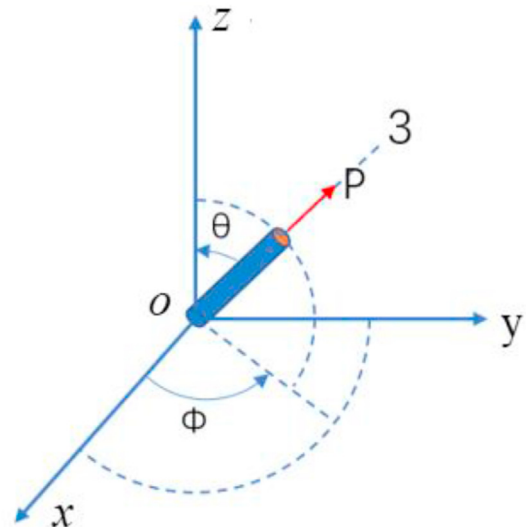


Fig. 2 – Angles to describe a CNT orientation in a 3D configuration.

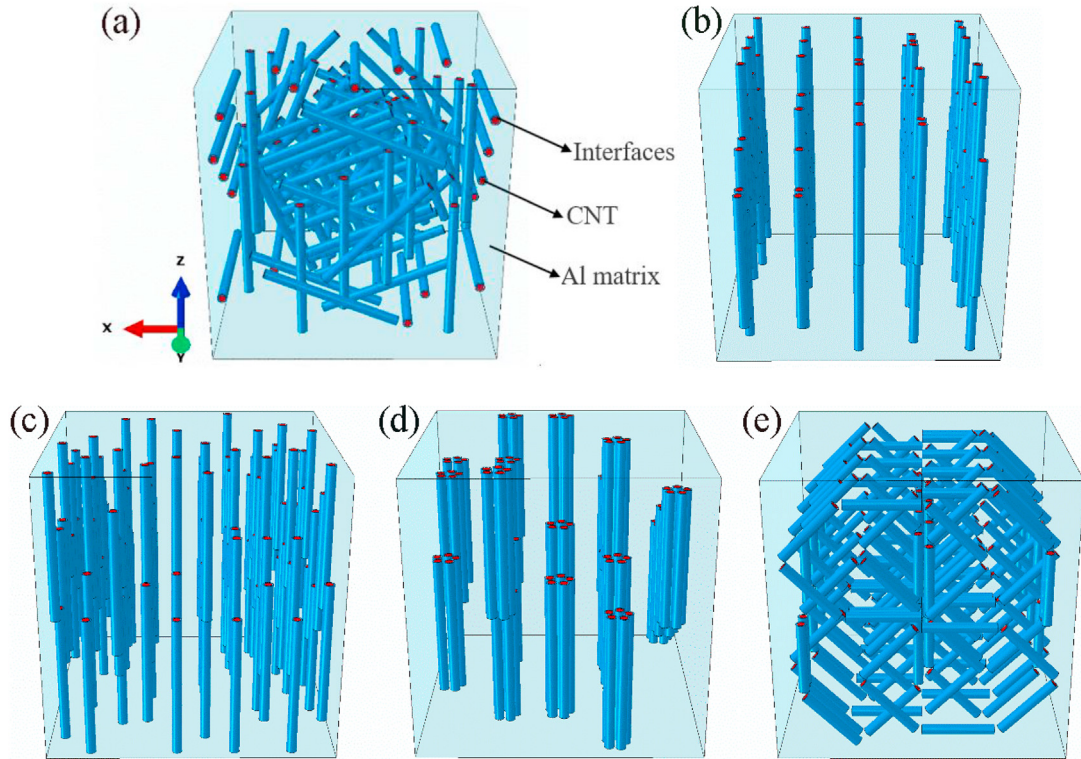


Fig. 3 – Schematics of RVE with five configurations of CNTs: (a) randomly arranged, (b) evenly oriented, (c) layered, (d) bundled, (e) networked.

3. Finite element analysis

In this work, the fully coupled temperature-displacement analysis was created for simulation of the thermal expansion behavior of CNT/Al composites. The geometrical models of CNT/Al composites are shown in Fig. 3, including five typical CNT configurations, namely randomly arranged, evenly oriented, layered, bundled and networked.

Fig. 3 illustrates the microstructure of 3D CNT/Al composites, consisting of Al matrix, CNTs and interfaces. The light-blue, red and deep-sky-blue in Fig. 3 represent Al matrix, CNTs and interfaces, respectively. In the figure, the red is the CNT and the blue is the interface. CNTs are one-dimensional nanomaterials with hollow cylinder formed by

curling graphite structure composed of six rings. Therefore, both of CNTs and interfaces are hollow cylinders. For simplicity, CNTs are simulated as a transversely isotropic solid cylinder with 10 nm diameter and 200 nm length, respectively, and each RVE includes 100 CNTs. As well known, the in-situ formation of interface (Al_4C_3) would occur on the outer surface of CNTs due to the interaction of C atoms with Al matrix, and the Al_4C_3 regions on the CNT surface can reach ~750 nm in length with a thickness of ~5 nm [27]. Therefore, the interface between CNT and surrounding matrix is modeled as a hollow cylinder with a thickness of 3 nm and of the same length as that of CNT, and the perfect

Table 1 – Material properties used in the finite element analysis [28,29,30,31,32].

Properties	Parameter	CNTs	Aluminum	Al_4C_3
Elastic properties	$E_1 = E_2$ (MPa)	298000	69000	72000
	E_3 (MPa)	952000	69000	72000
	$\nu_{12} = \nu_{21}$	0.419	0.35	0.33
	$\nu_{13} = \nu_{23}$	0.165	0.35	0.33
	$\nu_{31} = \nu_{32}$	0.425	0.35	0.33
	G_{12} (MPa)	105000	25555	27068
	$G_{13} = G_{23}$ (MPa)	408000	25555	27068
CTE	$\alpha_1 = \alpha_2$ ($10^{-6}/^\circ C$)	0	21.5	7.6
	α_3 ($10^{-6}/^\circ C$)	-12	21.5	7.6

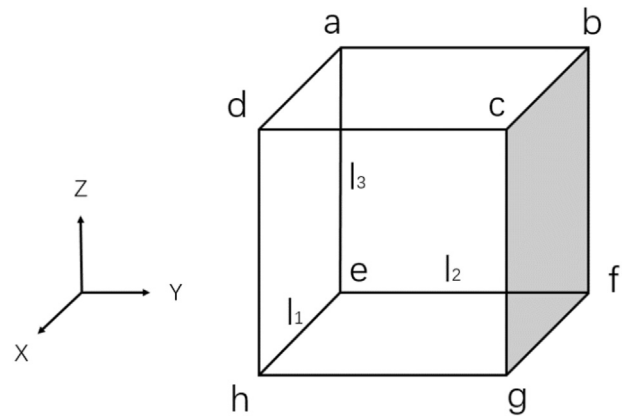


Fig. 4 – Unit cell model containing six boundary surfaces.

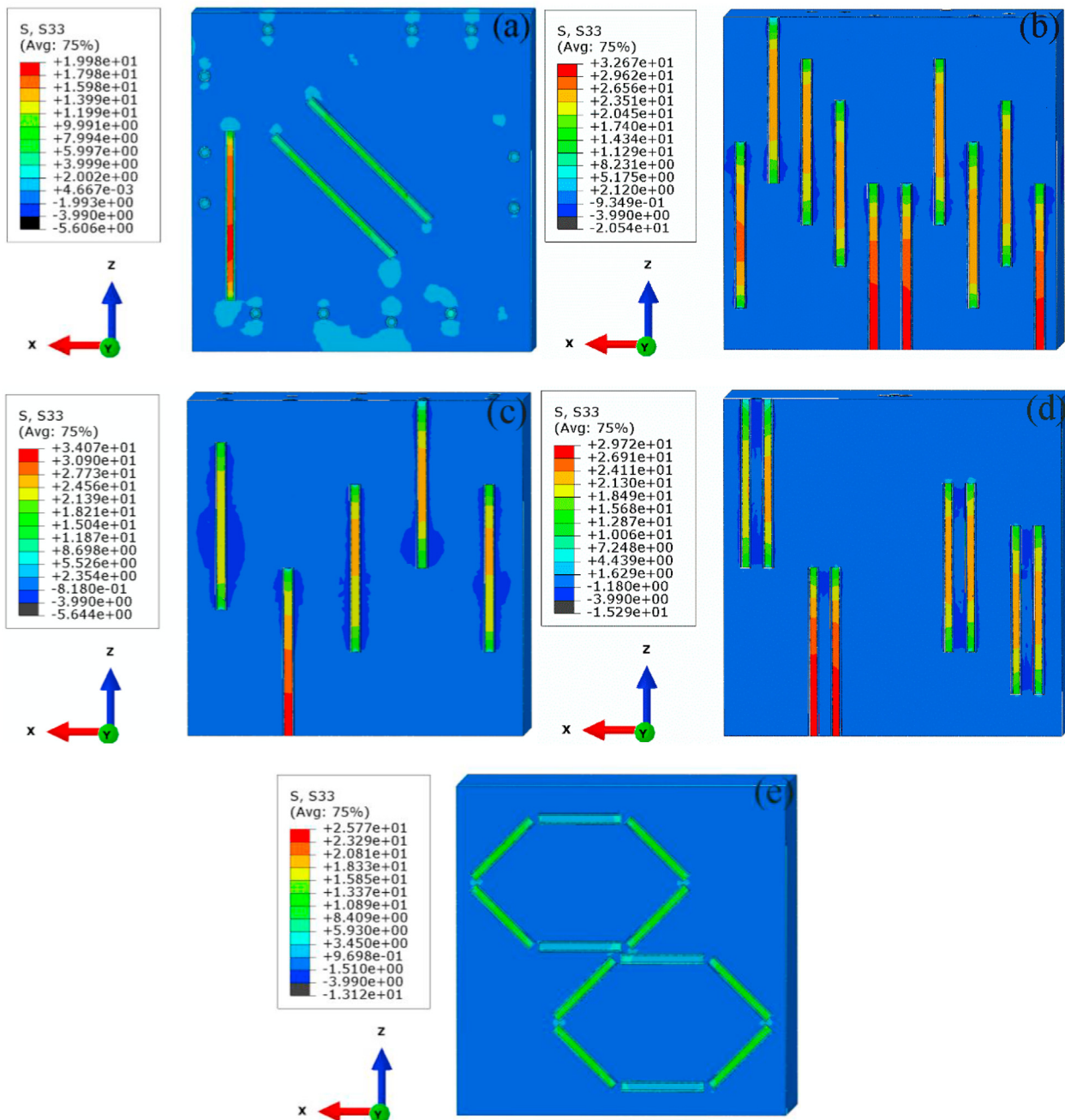


Fig. 5 – Stress distributions of CNT/Al composites: (a) randomly arranged, (b) evenly oriented, (c) layered, (d) bundled and (e) networked.

bonding between the interface and CNT has been assumed. The size of the RVE was $400 \text{ nm} \times 400 \text{ nm} \times 400 \text{ nm}$, and the volume fraction of CNTs is 3% for CNT/Al composites. Due to the difficulty in dispersing CNT in Al alloys, the volume fraction of CNTs in composites is usually selected under 5% or so. Some investigations have reported that the good comprehensive properties could be obtained for CNTs volume fraction of about 3% [1,6,12]. CNTs are assumed to be linearly elastic and transversely isotropic, while the matrix and

interfaces are assumed to be linearly thermoelastic and isotropic. The normalized thermoelastic properties used in the finite element analysis are given in Table 1 [28–32].

The geometry is meshed by 4-noded linear tetrahedral heat transfer elements (DC3D4), and the mesh size of 5 nm is selected for all the calculations. RVE with the periodic displacement boundary conditions under a uniform temperature change loading can be used to calculate the effective CTE [33]. In the process, the boundary surfaces of the

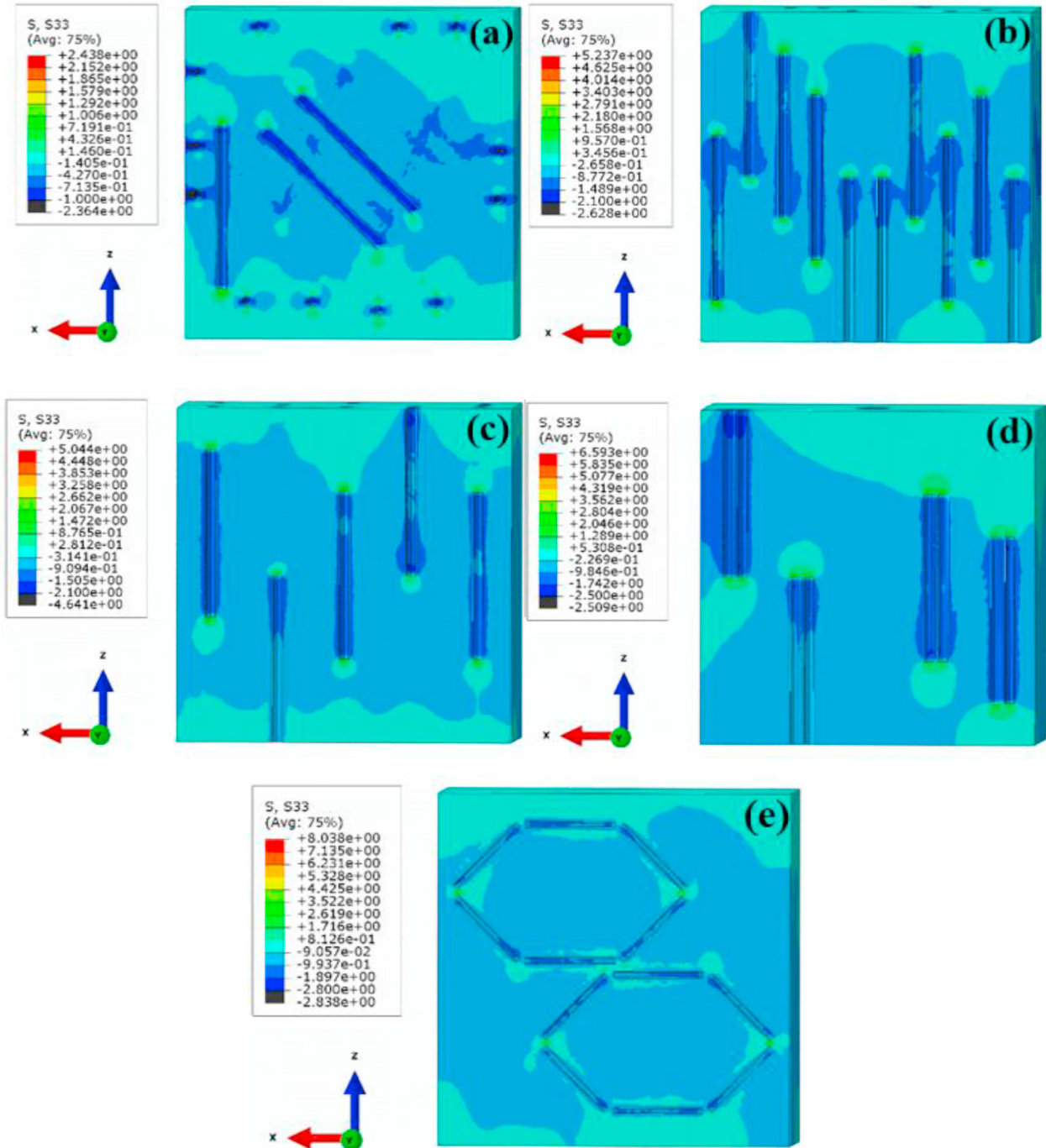


Fig. 6 – Stress distributions of Al matrix: (a) randomly arranged, (b) evenly oriented, (c) layered, (d) bundled and (e) networked.

neighboring cell should satisfy the strain continuity and the temperatures distributed at the opposite parallel node pairs must be uniform. Fig. 4 shows the unit cell model containing six boundary surfaces. Using three concurrent edges of the RVE to indicate the axes of the Cartesian coordinate system xyz, the applied periodic boundary conditions are written as follows:

$$\begin{cases} u_{dcgh} - u_{abfe} = l_1 \varepsilon_x = l_1 \alpha_x \Delta T \\ v_{cbfg} - v_{daeh} = l_2 \varepsilon_y = l_2 \alpha_y \Delta T \\ w_{abcd} - w_{efgh} = l_3 \varepsilon_z = l_3 \alpha_z \Delta T \end{cases} \quad (10)$$

where u, v and w are the displacements along x, y and z directions, respectively. u_{dcgh} is the displacement of each node on the boundary surface S_{dcgh} , etc. l_1, l_2 and l_3 are the lengths of RVE along x, y and z directions, respectively. ΔT

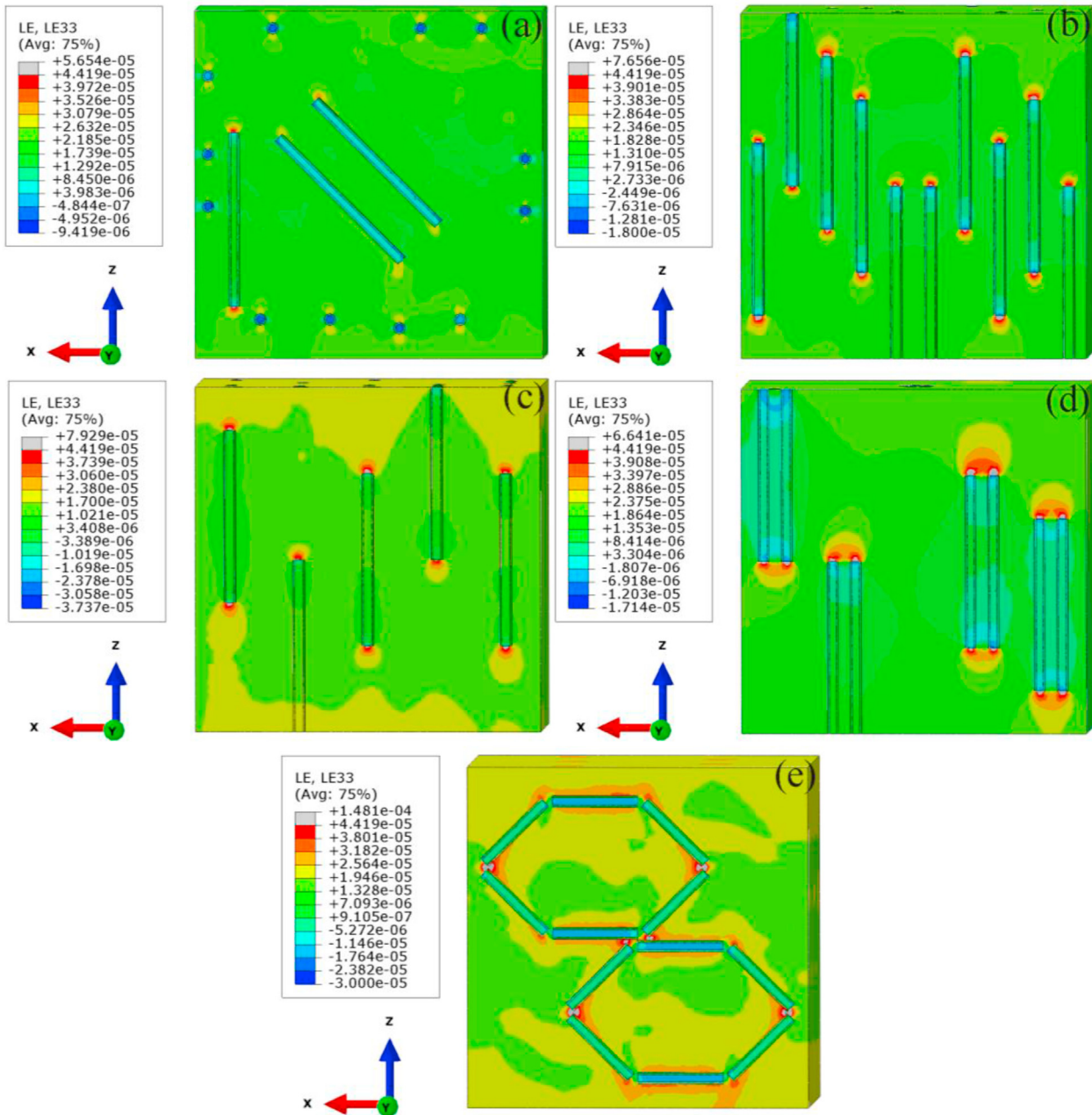


Fig. 7 – Strain distributions CNT/Al composites: (a) randomly arranged, (b) evenly oriented, (c) layered, (d) bundled and (e) networked.

is the temperature difference loading from the reference temperature.

4. Results and discussion

4.1. Stress and strain distributions

Fig. 5 shows the stress distributions along the z direction with $\Delta T = 1^\circ\text{C}$. It can be observed that the compression stress

(negative values) is localized in the matrix, while CNTs and interface underwent the tensile stress. The absolute stress values of CNTs are obviously higher than those of matrix and interface layer, and the tensile stress of CNTs parallel to the z axis is the highest. This is attributed to the anisotropy of CNTs and the mismatch of CTE between the matrix and CNTs. Meanwhile, for CNTs parallel to the load direction and close to the bottom of RVE, due to the constraint conditions of the symmetry plane, the tensile stress near to the symmetry plane is the highest, which is about 30 MPa. On the contrary,

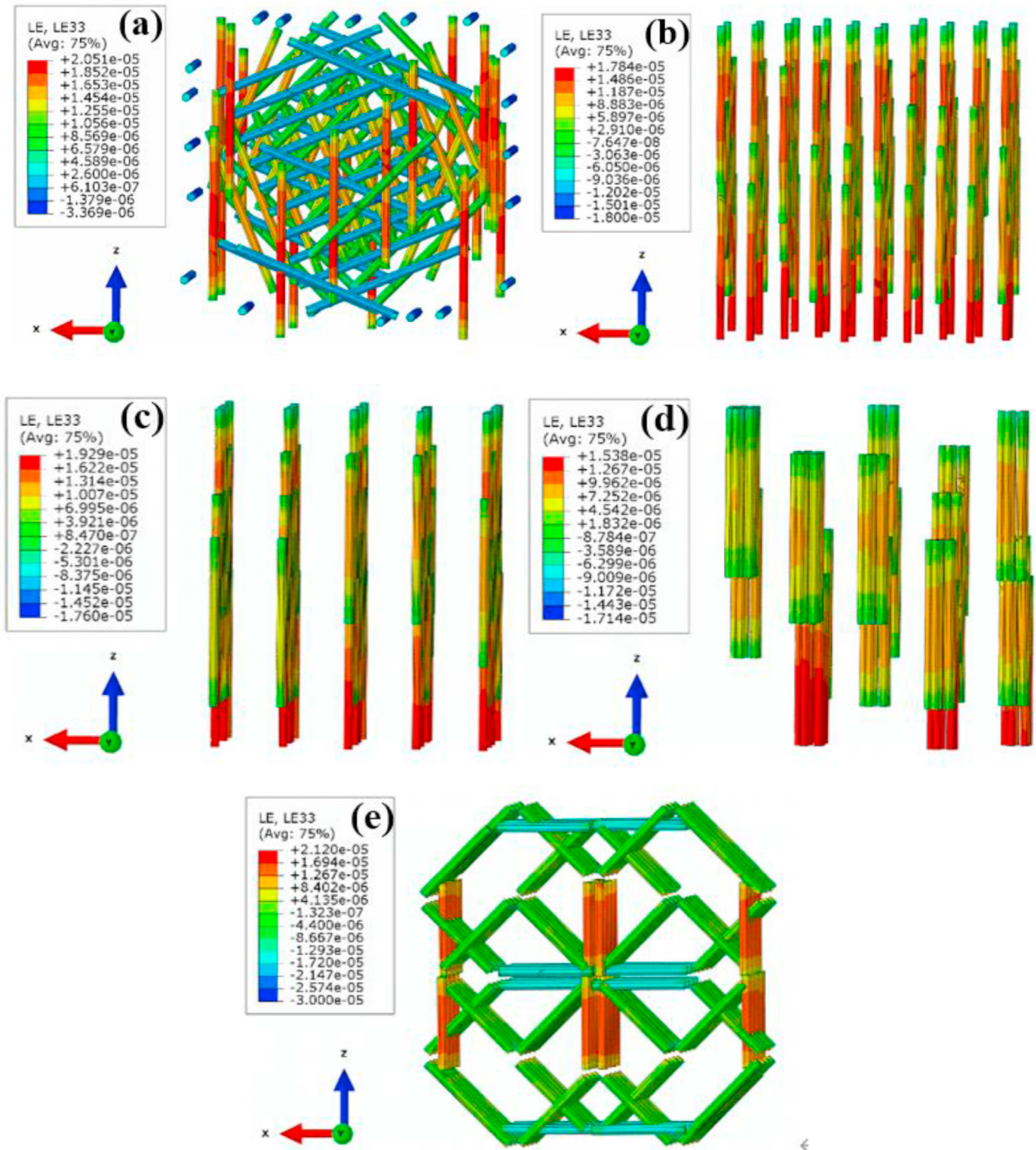


Fig. 8 – Strain distributions of CNTs: (a) randomly arranged, (b) evenly oriented, (c) layered, (d) bundled and (e) networked.

for CNTs far from the constraint surface, the tensile stress decreases gradually from the middle to both ends.

It is well known that the elastic modulus of CNT is much higher than that of Al matrix, and the stress value of matrix is almost the same in Fig. 5. However, due to the existence of different configurations of CNTs, the stress distribution of the

matrix without CNTs and interface is very irregular, as shown in Fig. 6. Obviously, most of the matrix underwent the compressive stress, and the absolute values where CNTs located is slightly higher than that of the other areas. The absolute value of the highest stress is only 2 MPa, which is much lower than that of CNT (see Fig. 5). What's more, the

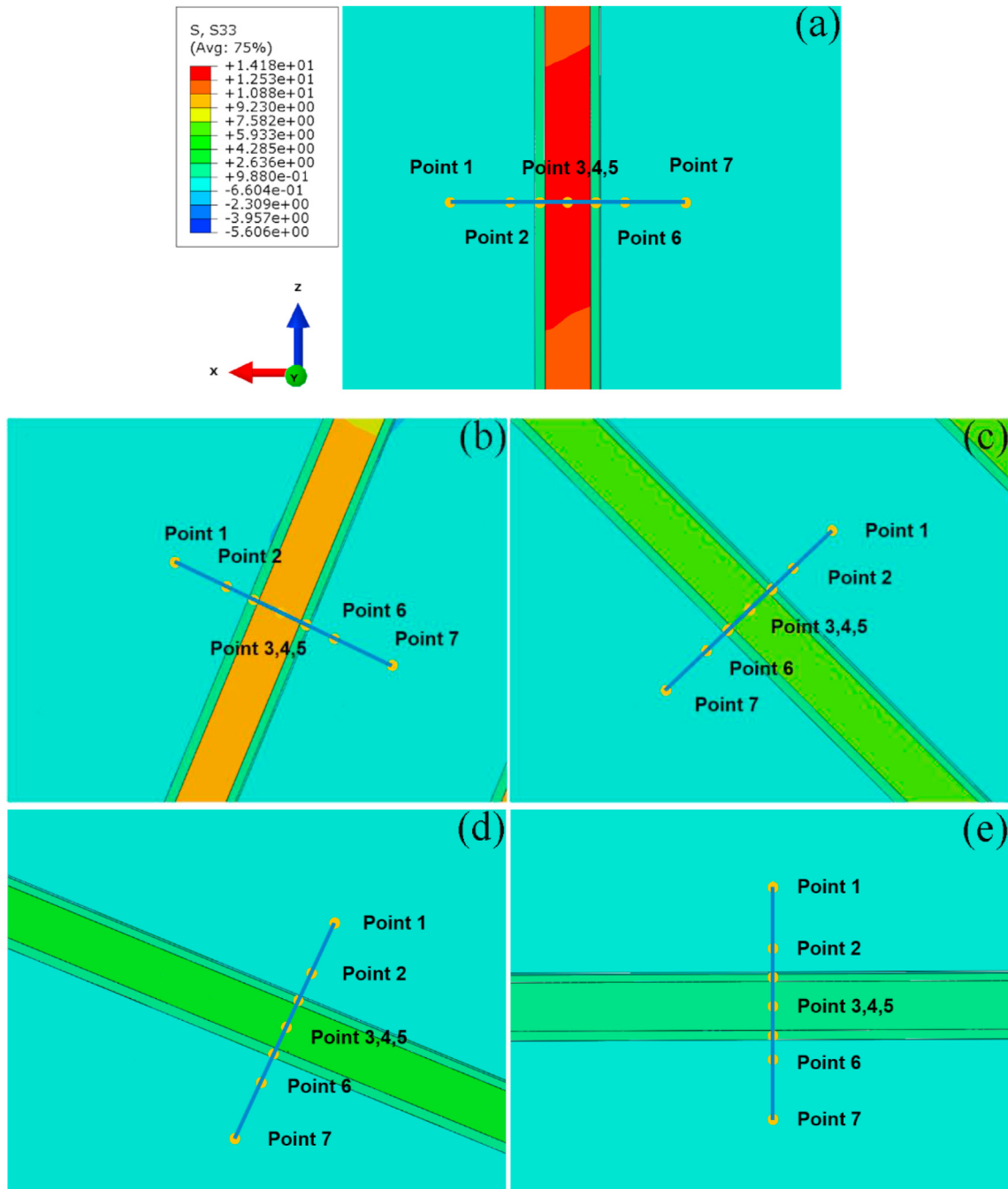


Fig. 9 – Local internal stress distributions with CNT orientations of (a) 0° , (b) 22.5° , (c) 45° , (d) 67.5° and (e) 90° .

configuration of CNTs has a little influence on the stress value of the matrix, the reason is that the volume fraction of CNTs is low.

Fig. 7 shows the strain distributions of CNT/Al composites along the z direction for five configurations. Different from that of the stress distribution, the matrix strain is significantly higher than that of the CNTs and interface. It can be also observed that after heating, the large strain gradient occurs mainly in the CNT/matrix interface zones along the axial

direction. The reason is that the axial direction CTE of CNTs is much lower than that of radial direction, and the constraint of CNTs on the matrix is the largest in the axial direction. Therefore, the maximum strain appears on the matrix at both ends of CNTs parallel to the z direction.

Similarly, due to the deformation of CNTs is significantly lower than that of the matrix, the difference of CNTs strain is not obvious when the alignment direction of CNTs is different (see Fig. 7). Therefore, Fig. 8 shows the strain

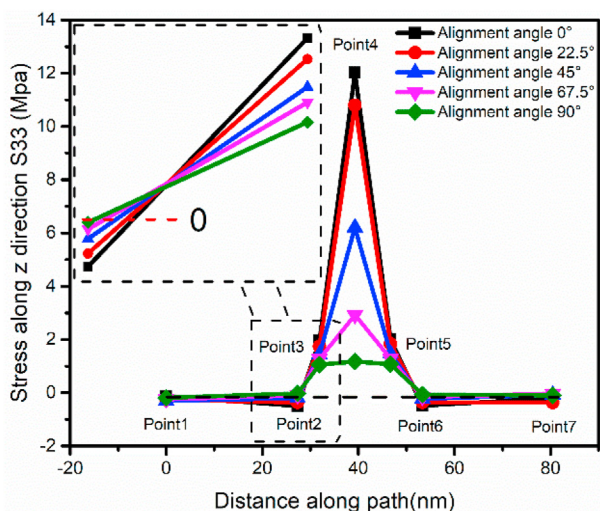


Fig. 10 – Stress values along five paths.

distributions of CNTs without interface and matrix for five configurations. It can be clearly seen that the strain distribution of CNTs without interface and matrix is also uneven, and the arrangement direction has the greatest influence on the strain of CNT. The strain is the highest when CNT is arranged along the direction of the load, and the maximum strain of CNT is about 2×10^{-5} , which is only half of the matrix strain.

4.2. Local stress and strain distributions

From Figs. 5–8, it is worth noting that the orientation of CNTs in the matrix has a great influence on the internal thermal stress and strain. Thus, five angles between the z axis positive direction and CNT are selected, that is 0° , 22.5° , 45° , 67.5° and 90° , respectively. Fig. 9 shows the local internal stress distribution of different CNT orientations in the RVEs. The path is perpendicular to CNT, from point 1 to point 7, and including positions in the matrix far from CNT and close to CNT, interface and CNT. Points 1 and 7 are the matrix stresses far away from CNT, points 2 and 6 are the matrix stresses near CNT, points 3 and 5 are the interface layer stresses, and point 4 is the CNT stress. From the figures, it can be observed that the stress of the matrix is much lower than that of CNT and not affected by the orientation of CNT. By contrast, the inclination angle has a great influence on the stress of CNT. The stress of CNT with angle of 0° is the largest (Fig. 9a), and with increasing CNT inclination angle, the stress decreases remarkably. When the CNT inclination angle is 90° , the stress value of CNT reaches the minimum (Fig. 9e). That is to say, when CNT is parallel to the load direction, the constraint effect of CNT on the matrix is the largest.

To quantitatively compare the internal stress of the different orientations of CNTs, Fig. 10 shows the stress variation for different points along the five paths. It is clear that the stress value of CNT decreases significantly with increasing the angle between CNT and z-axis. Indeed, the matrix stress values far away from CNT are almost the same,

as shown in points 1 and 7, and do not change with the change of CNT arrangement angle. On the contrary, the matrix stress values close to CNT are slightly different, as shown in points 2 and 6. From the local amplified figure of points 2 and 3, it can be noted that the stress value of point 2 slightly increases with the increase of the angle between the CNT and z axis, while the stress value of the interface layer decreases obviously (see local amplified figure of points 3). The stress variation of the interface layer is the same as that of CNT. This is due to the anisotropy of CNT along the axial and radial directions, and the different CTE of each component during thermal deformation.

Fig. 11 shows the local strain distribution with different arrangement angles of CNTs in RVE. Similarly, the paths include the matrix far from and close to CNT, interface and CNT. It is evident that the arrangement angle of CNT not only affects the strain of CNT, but also affects that of the interface and matrix. The strain values of CNT and interface show obvious sensitivity to the arrangement angle of CNT. With increasing the arrangement angle, the strains of CNT and interface decrease.

The strain values at different points along the five paths are shown in Fig. 12. In the same way, the path is perpendicular to CNT, including positions in the matrix far from CNT and close to CNT, interface and CNT. Points 1 and 7 are the matrix strain far away from CNT, points 2 and 6 are the matrix strain near CNT, points 3 and 5 are the interface strain, and point 4 is the CNT strain. It can be seen from the figure that the arrangement angle of CNT has a great influence on the strain values. Due to the very low CTE of CNT, the strain of CNT is the smallest during heating. With the increase of the angle between CNT and z-axis, the strain values of the interface layer and CNT decrease gradually. When the angle is 90° , the strain of the CNT and the interface reaches the minimum value. The influence of the alignment angle on the CNT strain is due to the anisotropy of CNT along the axial and radial directions, while the influence on the interface strain is the constrain to the thermal expansion by CNT. Although the interface layer is isotropic, its deformation trend is the same as that of CNT due to the perfect bonding between interface and CNT. Therefore, if the alignment direction of interface layer is along the load direction, the constrain on the deformation behavior of matrix is the most significant, which is beneficial to reduce the CTE of CNT/Al composites. Moreover, owing to the large CTE of the matrix, the strain of matrix is the highest and increases slightly with the increase of the angle between CNT and z axis.

4.3. CTE of CNT/Al composites

The CTE of CNT/Al composites for five configurations is calculated by using Eq. (1), and the variations of CTE are shown in Fig. 13. The horizontal axis represents five configurations of CNT, here, '1', '2', '3', '4' and '5' represent randomly arranged, evenly oriented, layered, bundled and networked configurations, respectively. From the figure it is evident that the CTE of CNT/Al composites decreased remarkably compared with that of Al matrix. In addition, the CTE of CNT/Al composites with bundled configuration is the lowest,

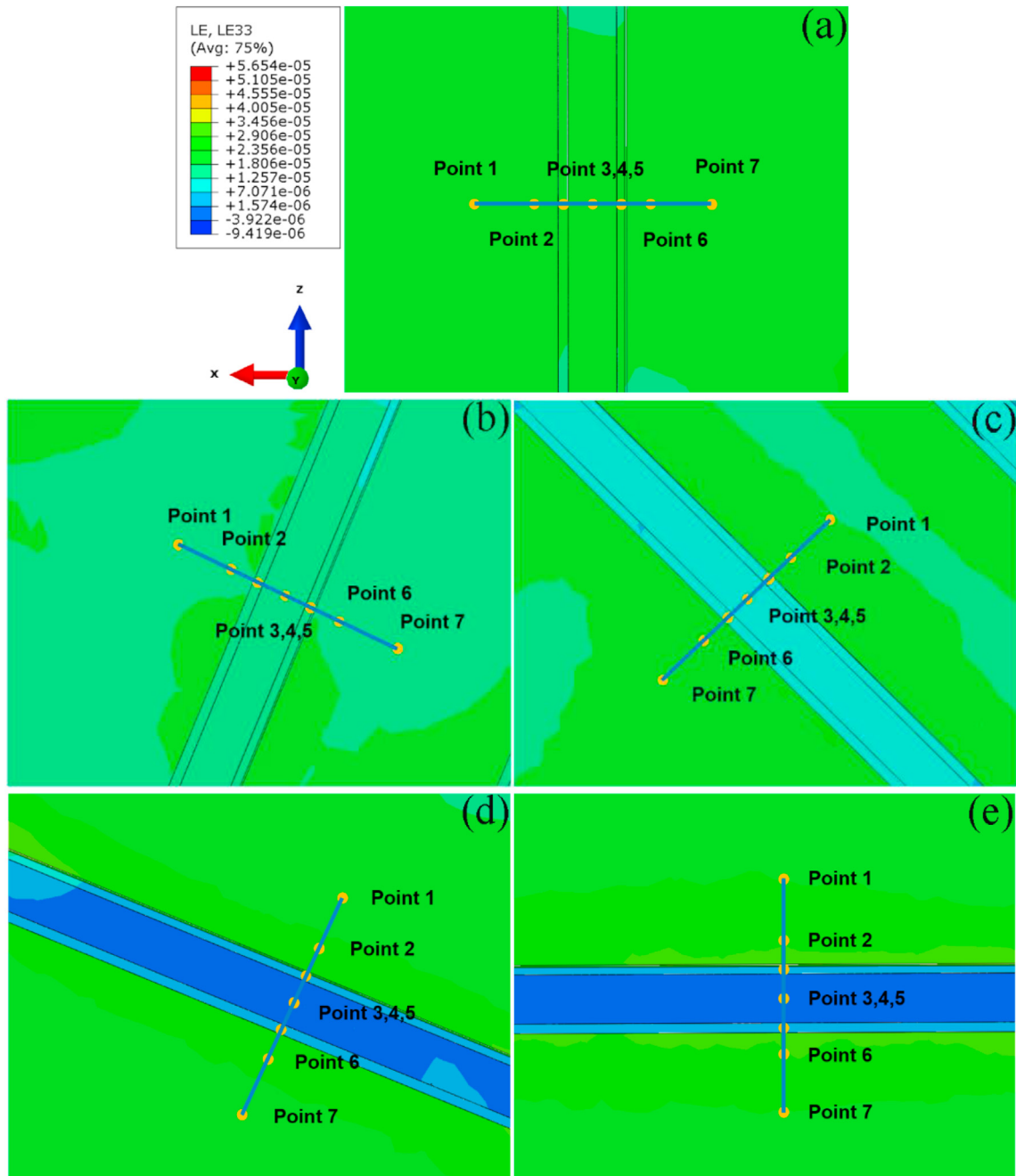


Fig. 11 – Local internal strain distributions with CNT orientations of (a) 0°, (b) 22.5°, (c) 45°, (d) 67.5° and (e) 90°.

followed by the evenly oriented and layered distribution. However, the CTEs for random and networked configurations are 16.75 and $15.58 \times 10^{-6}/^{\circ}\text{C}$, and the declines are not very obvious. This indicates that CNTs could effectively constrain the thermal expansion of the Al matrix when CNTs are well aligned in the matrix. On the contrary, the randomly arranged and networked configurations of CNTs cannot restrict the expansion of the matrix in a specific direction, which leads to high CTE. Therefore, the orientation and configuration of CNTs are very important factors that strongly affect the CTE of CNT/Al composites.

The CTE of bundled configuration CNT/Al composites is $11.86 \times 10^{-6}/^{\circ}\text{C}$, which decreases by about 45% compared with that of Al matrix. This indicates that the CNT could effectively constrain the thermal expansion of Al matrix, thereby resulting in a decline in the CTE of the composites.

4.4. Influence of volume fraction of CNTs

It is well known that the volume fraction of CNTs is the main factor that affects the mechanical and thermal properties of CNT/Al composites. Due to the lowest CTE of CNT/Al

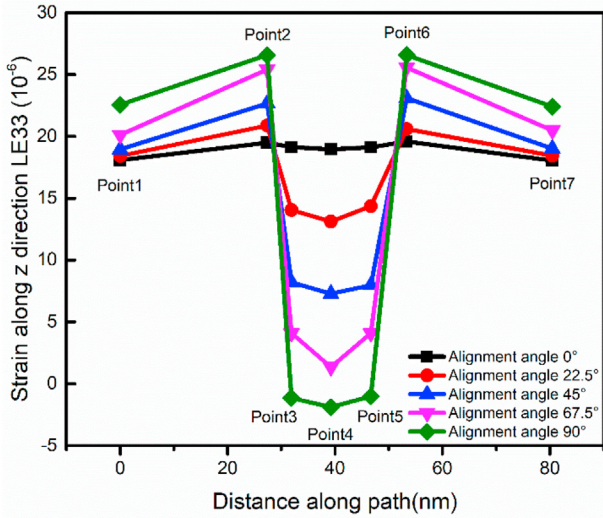


Fig. 12 – Strain values along five paths.

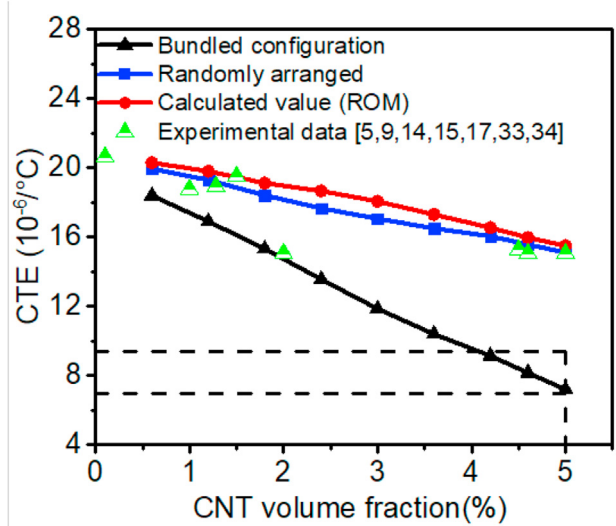


Fig. 14 – CTE of CNT/Al composites as a function of CNT volume fraction.

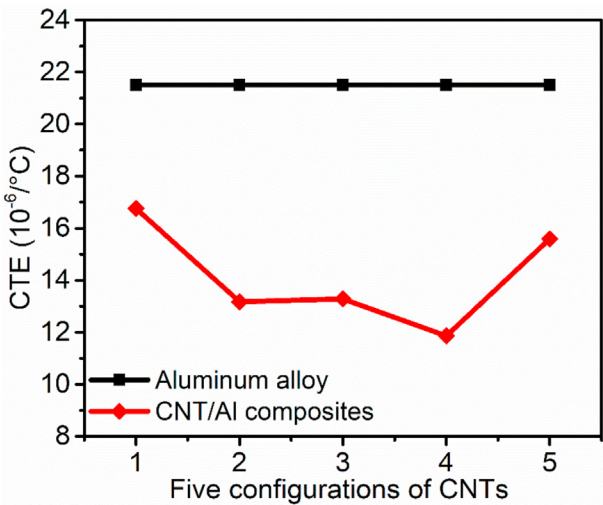


Fig. 13 – CTE comparison between RVE numerical models.

composites with bundled configuration, the RVE of bundled configuration is selected for investigating the influence of CNT volume fraction on the CTE. In this section, the volume fraction of CNTs is increased by increasing the number of bundles in RVE. The number of CNTs in each bundle is 5, and the bundled CNTs are uniformly dispersed in the matrix. Fig. 14 shows the CTE of CNT/Al composites with different volume fractions of CNTs. It is observed that the CTE decreases rapidly with CNT addition in the Al matrix. When the volume fraction of CNTs is 5%, the CTE reaches $7.2 \times 10^{-6}/^{\circ}\text{C}$ for the CNT/Al composites, and the CTE of the CNT/Al composites is 66% lower than the CTE of the matrix material.

To validate the numerical model of CNT/Al composites, the rule of mixtures (ROM) is used for calculating the CTE of the composites. Since the ROM cannot consider the orientation

and distribution of CNTs in the matrix, the CTE of CNT/Al composites with random configuration and experimental data from different literatures [5,9,14,15,17,33,34] are also shown in Fig. 14. It is clear that the CTE of CNT/Al composites with bundled configuration is much lower than those of the calculated theoretically and experimental. Moreover, the CTE of CNT/Al composites with random configuration is on a similar level with calculated theoretically and experimental values. Also, it is worth noting that the CTEs of randomly arranged are a little lower than those calculated by ROM. The reason is that the ROM is an approximation of a two-phase mixture, which does not take into account the presence of interface layer. Therefore, the FEM can consider the configuration, distribution and aggregation of CNTs in the matrix, and predict the CTE of CNT/Al composites more accurate.

4.5. Influence of bundled structure feature

CNTs are usually packed into bundles by van der Waals forces to form a close-packed bundle or array [35–37]. Thus, the structure feature of CNT bundle is one of the keys influencing the thermal performance of CNT/Al composites. To investigate the influence of CNT structure feature on the CTE, 5 different bundle structures were constructed, as shown in Fig. 15. Here, a total CNT number of 200 is adopted, and CNTs are vertically aligned for the bundle construction. Each bundle contains 5, 10, 15, 20 and 25 CNTs, respectively. Fig. 15a and b show the structure feature of bundled CNTs and its cross-section, for discussion convenience, the bundled CNTs are denoted as A, B, C, D and E, respectively. It is noteworthy that CNTs need to keep a certain distance from each other during establishing the RVE of bundled structure.

Fig. 16 shows the variation of CTE of CNT/Al composites with the number of CNTs for each bundle, and the five RVEs are calculated. With increasing the number of CNTs in each bundle, the CTE decreases and then follows a trend towards

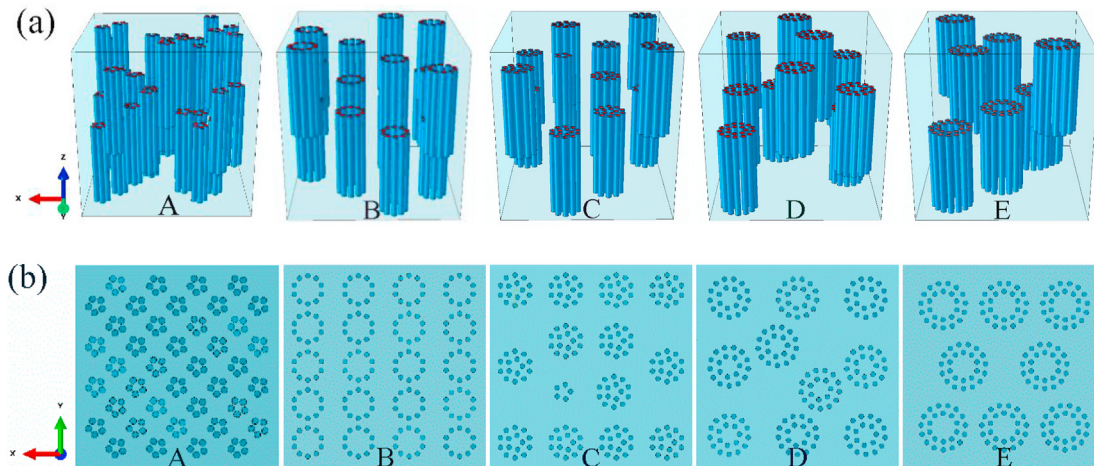


Fig. 15 – Morphology of bundled structure (a) axial view, and (b) cross-sectional view.

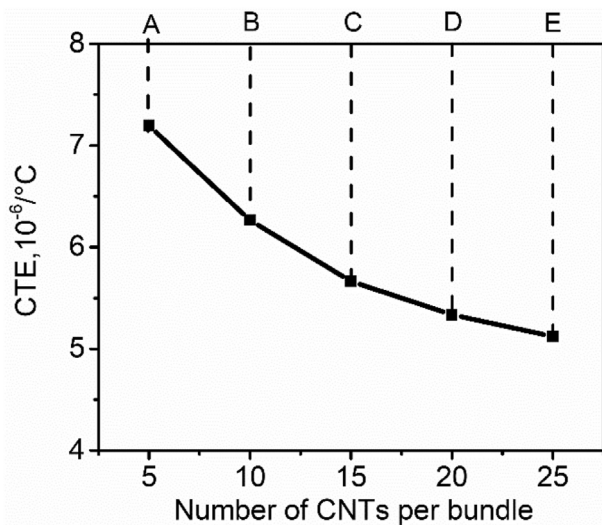


Fig. 16 – Variation of CTE of with the number of CNTs for each bundle.

unchanged around a bundle number larger than 20. When the volume fraction of CNTs is 5%, and the number of CNTs in each bundle is 25, the CTE of the composite reaches $5.12 \times 10^{-6}/^{\circ}\text{C}$, which is 76% lower than the CTE of the matrix.

5. Conclusions

- 1) Due to the anisotropy of CNT and the mismatch of CTE between the matrix and CNT, the orientation of CNT significantly influences the stress and strain. When CNT is parallel to the load direction, the constraint effect of CNT on the matrix is the largest.
- 2) The configuration of CNTs in the matrix plays an important role in reducing the CTE of CNT/Al composites, and the CTE

of the bundled configuration is the lowest compared with that of the other configurations. In addition, with the increase of the number of CNTs in each bundle, the CTE of CNT/Al composites decreases and then tends to be unchanged. When the volume fraction of CNTs is 5%, and the number of CNTs in each bundle is 25, the CTE of the composite reaches $5.12 \times 10^{-6}/^{\circ}\text{C}$, which is 76% lower than the CTE of the matrix.

- 3) The effect of increasing the volume fraction of CNTs leads to the decrease in the CTE of CNT/Al composites remarkably. The CTE of CNT/Al composites with random configuration is on a similar level with calculated theoretically and experimental values. Therefore, the FEM in this work can predict the CTE of CNT/Al composites more accurate.

Declaration of Competing Interest

The authors declare that they have no known competing financial interests or personal relationships that could have appeared to influence the work reported in this paper.

Acknowledgements

This research is financially supported by the National Natural Science Foundation of China (No. 51871214, 51931009 and 51871215) and Key Research Program of Frontier Sciences, CAS (No. QYZDJ-SSW-JSC015).

REFERENCES

- [1] Shin SE, Ko YJ, Bae DH. Mechanical and thermal properties of nanocarbon-reinforced aluminum matrix composites at elevated temperatures. *Compos B Eng* 2016;106:66–73.

- [2] Khanna N, Suri NM, Shah P, Hegab H, Mia M. Cryogenic turning of in-house cast magnesium based MMCs: a comprehensive investigation. *J Mater Res Technol* 2020;9:7628–43.
- [3] Zhan JM, Yao XH, Han F, Zhang XQ. A rate-dependent peridynamic model for predicting the dynamic response of particle reinforced metal matrix composites. *Compos Struct* 2021;263:113673.
- [4] Wang MM, Yang JS, You X, Liao CJ, Yan JY, Ruan J, et al. Nanoinfiltration behavior of carbon nanotube based nanocomposites with enhanced mechanical and electrical properties. *J Mater Sci Technol* 2021;71:23–30.
- [5] Liu ZY, Xiao BL, Wang WG, Ma ZY. Developing high-performance aluminum matrix composites with directionally aligned carbon nanotubes by combining friction stir processing and subsequent rolling. *Carbon* 2013;62:35–42.
- [6] Yang X, Zou T, Shi C, Liu E, He C, Zhao N. Effect of carbon nanotube (CNT) content on the properties of in-situ synthesis CNT reinforced Al composites. *Mater Sci Eng* 2016;660:11–8.
- [7] Yetgin SH. Effect of multi walled carbon nanotube on mechanical, thermal and rheological properties of polypropylene. *J Mater Res Technol* 2019;8:4725–35.
- [8] B Li P, Yang H, M Gao M. Microstructure and mechanical properties of multi-scale in-situ Mg₂Si and CNTs hybrid reinforced AZ91D composites. *J Mater Res Technol* 2021;14:2471–85.
- [9] Shirasu K, Nakamura A, Yamamoto G, Ogasawara T, Shimamura Y, Inoue Y, et al. Potential use of CNTs for production of zero thermal expansion coefficient composite materials: an experimental evaluation of axial thermal expansion coefficient of CNTs using a combination of thermal expansion and uniaxial tensile tests. *Compos Part A Appl Sci Manuf* 2017;95:152–60.
- [10] Simões S, Viana F, Reis MAL, Vieira MF. Influence of dispersion/mixture time on mechanical properties of Al–CNTs nanocomposites. *Compos Struct* 2015;126:114–22.
- [11] Liu ZY, Xiao BL, Wang WG, Ma ZY. Elevated temperature tensile properties and thermal expansion of CNT/2009Al composites. *Compos Sci Technol* 2012;72:1826–33.
- [12] Esawi AMK, Morsi K, Sayed A, Taher M, Lanka S. Effect of carbon nanotube (CNT) content on the mechanical properties of CNT-reinforced aluminium composites. *Compos Sci Technol* 2010;70:2237–41.
- [13] Liu ZY, Xiao BL, Wang WG, Ma ZY. Effect of carbon nanotube orientation on mechanical properties and thermal expansion coefficient of carbon nanotube-reinforced aluminum matrix composites. *Acta Metall Sin Engl Lett* 2014;27:901–8.
- [14] Murugesan R, Gopal M, Murali G. Effect of Cu, Ni addition on the CNTs dispersion, wear and thermal expansion behavior of Al-CNT composites by molecular mixing and mechanical alloying. *Appl Surf Sci* 2019;495:143542.
- [15] Trinh PV, Luan NV, Phuong DD, Minh PN, Weibel A, Mesguich D, et al. Microstructure, microhardness and thermal expansion of CNT/Al composites prepared by flake powder metallurgy. *Compos Part A Appl Sci Manuf* 2018;105:126–37.
- [16] Sharma M, Sharma V. Chemical, mechanical, and thermal expansion properties of a carbon nanotube-reinforced aluminum nanocomposite. *Int. J. Miner. Metall. Mater.* 2016;23:222–33.
- [17] Tang YB, Cong HT, Zhong R, Cheng HM. Thermal expansion of a composite of single-walled carbon nanotubes and nanocrystalline aluminum. *Carbon* 2004;42:3251–72.
- [18] Deng CF, Ma YX, Zhang P, Zhang XX, Wang DZ. Thermal expansion behaviors of aluminum composite reinforced with carbon nanotubes. *Mater Lett* 2008;62:2301–3.
- [19] Millen SLJ, Ullah Z, Falzon BG. On the importance of finite element mesh alignment along the fibre direction for modelling damage in fibre-reinforced polymer composite laminates. *Compos Struct* 2021;278:114694.
- [20] Shokrieh MM, Rafiee R. A review of the mechanical properties of isolated carbon nanotubes and carbon nanotube composites. *Mech Compos Mater* 2010;46:155–72.
- [21] Yang L, Miyoshi Y, Sugio K, Choi Y, Matsugi K, Sasaki G. Effect of graphite orientation distribution on thermal conductivity of Cu matrix composite. *Mater Chem Phys* 2021;257:123702.
- [22] Chen JF, Yan LX, Liang SY, Cui XP, Liu CN, Wang BS, et al. Remarkable improvement of mechanical properties of layered CNTs/Al composites with Cu decorated on CNTs. *J Alloys Compd* 2022;901:163404.
- [23] Jiang L, Li ZQ, Fan GL, Cao LL, Zhang D. Strong and ductile carbon nanotube/aluminum bulk nanolaminated composites with two-dimensional alignment of carbon nanotubes. *Scripta Mater* 2012;66:331–4.
- [24] Ashish S, Rajeevan C, Rohit D. Proposal and analysis of relative stability in mixed CNT bundle for sub-threshold interconnects. *Integration* 2021;80:29–40.
- [25] Mirkhalaf SM, Eggels EH, van Beurden TJH, Larsson F, Fagerstrom M. A finite element based orientation averaging method for predicting elastic properties of short fiber reinforced composites. *Compos B Eng* 2020;202:108388.
- [26] Chao XJ, Qi LH, Tian WL, Lu YF, Li HJ. Potential of porous pyrolytic carbon for producing zero thermal expansion coefficient composites: a multi-scale numerical evaluation. *Compos Struct* 2020;235:111819.
- [27] Zhou WW, Bang S, Kurita H, Miyazaki T, Fan YC. Interface and interfacial reactions in multi-walled carbon nanotube reinforced aluminum matrix composites. *Carbon* 2016;96:919–28.
- [28] Arora G, Pathak H. Modeling of transversely isotropic properties of CNT-polymer composites using meso-scale FEM approach. *Compos B Eng* 2019;166:588–97.
- [29] Chen X, Alian AR, Meguid SA. Modeling of CNT-reinforced nanocomposite with complex morphologies using modified embedded finite element technique. *Compos Struct* 2019;227:111329.
- [30] Sadeghi B, Qi JS, Min XR, Cavaliere P. Modelling of strain rate dependent dislocation behavior of CNT/Al composites based on grain interior/grain boundary affected zone (GI/GBAZ). *Mater Sci Eng, A* 2021;820:141547.
- [31] Zhang XX, Zhang JF, Liu ZY, Gan WM, Hofmann M, Andra H, et al. Microscopic stresses in carbon nanotube reinforced aluminum matrix composites determined by in-situ neutron diffraction. *J Mater Sci Technol* 2020;54(19):58–68.
- [32] J Tan Z, Li JY, Zhang Z. Experimental and numerical studies on fabrication of nanoparticle reinforced aluminum matrix composites by friction stir additive manufacturing. *J Mater Res Technol* 2021;12:1898–912.
- [33] Liu XD, Guan ZD, Wang XD, Jiang T, Geng KH, Li ZS. Improved semi-analytical and numerical methods on prediction of in-plane coefficients of thermal expansion of woven ceramic matrix composite considering defects. *J Eur Ceram Soc* 2021;41:1795–809.
- [34] Aborkin AV, Elkin AI, Reshetniak VV, Ob'edkov AM, Sytschev AE, Leontiev VG, et al. Thermal expansion of aluminum matrix composites reinforced by carbon nanotubes with in-situ and ex-situ designed interfaces ceramics layers. *J Alloys Compd* 2021;872:159593.
- [35] Cranford S, Yao HM, Ortiz C, Buehler MJ. A single degree of freedom 'lollipop' model for carbon nanotube bundle formation. *J Mech Phys Solid* 2010;58:409–27.
- [36] Kis A, Csányi G, Salvétat J-P, Lee Thien-Nga, Coureau E, Kulik AJ, et al. Reinforcement of single-walled carbon nanotube bundles by intertube bridging. *Nat Mater* 2004;3:153–7.
- [37] Liu Q, Li M, Gu YZ, Zhang YY, Wang SK, Li QW, et al. Highly aligned dense carbon nanotube sheets induced by multiple stretching and pressing. *Nanoscale* 2014;6:4338–44.